Downloaded from orbit.dtu.dk on: Oct 15, 2024

DTU Library

Rationally Designed PdAuCu Ternary Alloy Nanoparticles for Intrinsically Deactivation-Resistant Ultrafast Plasmonic Hydrogen Sensing

Darmadi, Iwan; Nugroho, Ferry Anggoro Ardy; Kadkhodazadeh, Shima; Wagner, Jakob B.; Langhammer, Christoph

Published in:
ACS Sensors

Link to article, DOI:
10.1021/acssensors.9b00610

Publication date:
2019

Document Version
Peer reviewed version

Link back to DTU Orbit

Citation (APA):
Darmadi, I., Nugroho, F. A. A., Kadkhodazadeh, S., Wagner, J. B., & Langhammer, C. (2019). Rationally Designed PdAuCu Ternary Alloy Nanoparticles for Intrinsically Deactivation-Resistant Ultrafast Plasmonic Hydrogen Sensing. *ACS Sensors*, *4*(5), 1424-1432. https://doi.org/10.1021/acssensors.9b00610

General rights
Copyright and moral rights for the publications made accessible in the public portal are retained by the authors and/or other copyright owners and it is a condition of accessing publications that users recognise and abide by the legal requirements associated with these rights.

- Users may download and print one copy of any publication from the public portal for the purpose of private study or research.
- You may not further distribute the material or use it for any profit-making activity or commercial gain
- You may freely distribute the URL identifying the publication in the public portal

If you believe that this document breaches copyright please contact us providing details, and we will remove access to the work immediately and investigate your claim.

ACS SENSORS

DTU Library
Technical Information Center of Denmark

Subscriber access provided by DTU Library

Article

Rationally-Designed PdAuCu Ternary Alloy Nanoparticles for Intrinsically Deactivation-Resistant Ultrafast Plasmonic Hydrogen Sensing

Iwan Darmadi, Ferry Anggoro Ardy Nugroho, Shima Kadkhodazadeh, Jakob B. Wagner, and Christoph Langhammer

ACS Sens., **Just Accepted Manuscript** • DOI: 10.1021/acssensors.9b00610 • Publication Date (Web): 06 May 2019

Downloaded from http://pubs.acs.org on May 9, 2019

Just Accepted

"Just Accepted" manuscripts have been peer-reviewed and accepted for publication. They are posted online prior to technical editing, formatting for publication and author proofing. The American Chemical Society provides "Just Accepted" as a service to the research community to expedite the dissemination of scientific material as soon as possible after acceptance. "Just Accepted" manuscripts appear in full in PDF format accompanied by an HTML abstract. "Just Accepted" manuscripts have been fully peer reviewed, but should not be considered the official version of record. They are citable by the Digital Object Identifier (DOI®). "Just Accepted" is an optional service offered to authors. Therefore, the "Just Accepted" Web site may not include all articles that will be published in the journal. After a manuscript is technically edited and formatted, it will be removed from the "Just Accepted" Web site and published as an ASAP article. Note that technical editing may introduce minor changes to the manuscript text and/or graphics which could affect content, and all legal disclaimers and ethical guidelines that apply to the journal pertain. ACS cannot be held responsible for errors or consequences arising from the use of information contained in these "Just Accepted" manuscripts.

ACS Publications

is published by the American Chemical Society. 1155 Sixteenth Street N.W., Washington, DC 20036

Published by American Chemical Society. Copyright © American Chemical Society. However, no copyright claim is made to original U.S. Government works, or works produced by employees of any Commonwealth realm Crown government in the course of their duties.

Rationally-Designed PdAuCu Ternary Alloy Nanoparticles for Intrinsically Deactivation-Resistant Ultrafast Plasmonic Hydrogen Sensing

Iwan Darmadi[1, ‡], *Ferry Anggoro Ardy Nugroho*[1, ‡], *Shima Kadkhodazadeh*[2], *Jakob B. Wagner*[2] *and Christoph Langhammer*[1,*]

[1]Department of Physics, Chalmers University of Technology, 412 96 Göteborg, Sweden

[2]Center for Electron Nanoscopy, Technical University of Denmark, 2800 Kongens Lyngby, Denmark

‡ these authors contributed equally

ABSTRACT

Hydrogen sensors are a prerequisite for the implementation of a hydrogen economy due to the high flammability of hydrogen-air mixtures. They are to comply with the increasingly stringent requirements set by stakeholders, such as the automotive industry and manufacturers of hydrogen safety systems, where sensor deactivation is a severe but widely unaddressed problem. In response, we report intrinsically deactivation-resistant nanoplasmonic hydrogen sensors enabled by a rationally-designed ternary PdAuCu alloy nanomaterial, which combines the identified best intrinsic attributes of the constituent binary Pd alloys. This way we achieve extraordinary hydrogen sensing metrics in synthetic air and poisoning gas background, simulating real application conditions. Specifically, we find a detection limit in the low ppm range, hysteresis-free response over 5 orders of magnitude hydrogen concentration, sub-second response time at room temperature, long-term stability and, as the key, excellent resistance to deactivating species like carbon monoxide, notably without application of any protective coatings. This constitutes an important step forward for optical hydrogen sensor technology, as it enables application under demanding conditions and provides a blueprint for further material and performance optimization by combining and concerting intrinsic material assets in multicomponent nanoparticles. In a wider context, our findings highlight the potential of rational materials design through alloying of multiple elements for gas sensor development, as well as the potential of engineered metal alloy nanoparticles in nanoplasmonics and catalysis.

Keywords: hydrogen sensor, nanoplasmonic sensor, nanofabrication, CO-resistance, carbon monoxide, palladium, copper

The hydrogen economy scenario[1] proposes the use of hydrogen gas as the next-generation energy carrier due to its high gravimetric energy density.[2] Furthermore, hydrogen only produces water as a byproduct during combustion or the electrochemical recombination with oxygen in a fuel cell. However, the widespread use of hydrogen fuel is complicated by its wide flammability range in air (4–75 *vol*.%) and by its low ignition energy (0.02 mJ), which impose a significant safety risk. Hence, any appliance or vehicle fueled by hydrogen, as well as the necessary distribution infrastructure, must be equipped with hydrogen sensors. Moreover, hydrogen sensors also find application in other sectors, such as industrial process monitoring and health diagnostics.[3–6] Among a variety of hydrogen sensors already available either at the R&D stage or commercially,[3,7–9] optical hydrogen sensors are particularly attractive since they pose little risk of spark generation due to remote readout capabilities by means of light. Within this field, nanoplasmonic hydrogen sensors utilizing the localized surface plasmon resonance (LSPR) in hydride-forming metal nanoparticles as signal transducer are rapidly developing.[10–19] They are intrinsically highly hydrogen selective since the hydrogen detection signal stems from the transition from the metallic to the metal hydride state *via* absorption of hydrogen into interstitial sites of the metal host.[10] Furthermore, their optical fingerprint is spectrally tunable,[11,16,20–22] they exhibit high sensitivities,[11,12,19,23] can be miniaturized down to the single nanoparticle level,[13,24–26] and are characterized by fast response due to the high surface-to-volume ratio of the active sensing entities.[11,14,19,27]

Driven by these unique prospects, numerous sensing nanoarchitectures have already been developed, but pure palladium (Pd) remains the primarily chosen material (exceptions exist, *e.g.* Mg,[21] Y,[22] Hf,[28] PdAu[11,14,15,19,27]) due to its ability to dissociate hydrogen gas efficiently at ambient conditions, and due to its reversible phase transformation from metal to metal

hydride.[10,29] In most other respects, however, Pd has significant shortcomings. For example, due to an energy barrier created by lattice strain during phase transformation, hysteresis between hydrogen absorption and desorption is observed[30] and hampers sensor uncertainty and dynamic range. Specifically, the sensor uncertainty is adversely affected since the response will depend on sensor history, and readout may thus be ambiguous. For example it has been shown previously that hysteretic behavior in Pd nanoparticles introduces readout uncertainty as high as 45% at ambient conditions.[11] On the other hand, the sensor dynamic range is also limited for Pd since it features a large response only in a very narrow hydrogen pressure range *i.e.* around the phase transformation in the mixed $\alpha + \beta$ phase region. To this end, the strategy of pre-straining the Pd lattice and thus lowering of the critical temperature *via* alloying with other metals with different lattice constants (*e.g.* Au, Ag, Ni) has been demonstrated to alleviate the limitations induced by hysteresis.[11,14,15,18,19,31,32] For the particular case of the PdAu alloy system, hysteresis-free response is obtained by alloying to 25 *at*.% Au. This facilitates a significant reduction of the readout uncertainty to below 5% throughout the 1–1000 mbar hydrogen pressure range.[11]

A second critical aspect of Pd-based hydrogen sensors (as well as of other emerging materials used for optical hydrogen sensing, *e.g.* Mg,[21] Y[22] or Hf[28] for which a Pd capping layer needs to be applied) is the fact that hydrogen dissociation is effectively poisoned even by trace amounts of gases like carbon monoxide (CO), sulfuric compounds (*e.g.* H_2S) and hydrocarbons.[7,8] In particular, CO is known to interfere with hydrogen sensors based on Pd,[3,33] on which it chemisorbs *via* its C atom and blocks hydrogen dissociation sites.[34–36] The favorable chemisorption of CO on Pd surfaces, as compared to other carbonaceous species such as CO_2 and CH_4, is due to its spatial atomic arrangement that provides a binding configuration at relatively low energy.[36,37] Deactivation by CO is thus problematic not only in applications where

the presence of CO is inevitable, such as during syngas production,[38] but also at ambient conditions due to its natural occurrence of *ca.* 0.2 ppm in air, and at higher concentrations close to large point sources or in urban areas.[39] Surprisingly, this explicit problem is only very rarely addressed in the large body of literature that reports on Pd-based hydrogen sensors.[7,8,10] To this end, to the best of our knowledge, only a handful of works discuss and report significant sensor resistance towards CO poisoning; and all achieve this function by applying a protection layer (*e.g.* polymers, metal-organic frameworks) that acts as H_2-selective filter on the Pd sensor.[19,40–42]

Here we present a different approach, which aims at rationally combining several beneficial *intrinsic* aspects of alloying Pd with *multiple* noble metals in order to eliminate hysteresis, increase sensor response time and create resistance to CO poisoning. Specifically, we set out to combine the CO-resistant properties of PdCu alloys[36,43–46] with the superior hydrogen sensing properties of PdAu alloys[11,14,15,47] by nanofabricating plasmonic PdAuCu *ternary* alloy nanoparticles with well-controlled composition. As we show, they feature unprecedented sensing metrics for a nanoplasmonic hydrogen sensor by combining the best attributes of the constituent binary alloy systems, *i.e.* a detection limit in the low ppm range, hysteresis-free response over 5 orders of magnitude hydrogen concentration, sub-second response time at room temperature and excellent long-term stability and resistance towards CO poisoning.

To fabricate our sensors, we used an approach of layer-by-layer deposition of tailored amounts of Cu, Au and Pd through a pre-fabricated hole-mask,[48] followed by thermal annealing,[15] to produce square centimeter quasi-random arrays of disk-shaped alloy nanoparticles with the desired composition (Figure S1). For the first part of our study, to benchmark the amount of Cu needed to obtain the required CO-poisoning resistance, we fabricated PdCu alloy nanoparticle arrays with different compositions ($Pd_{100-x}Cu_x$, x = 0–30 *at*.%, in steps of 5 *at*.%, which keeps us

below the threshold for fcc-bcc phase transitions[49]), while keeping the nominal diameter and thickness constant at 190 nm and 25 nm, respectively. Employing Scanning Transmission Electron Microscopy - Energy-Dispersive X-Ray Spectroscopy (STEM-EDS), we confirmed the formation of homogeneous alloys (**Figure 1**a and S2), which is also corroborated by the optical properties of the nanoparticles[15] (Figure S3). Furthermore, as we recently have demonstrated by combined plasmonic and quartz crystal microbalance (QCM) measurements,[16] a linear correlation between the spectral shift of the LPSR peak, $\Delta\lambda_{peak}$, and the Pd atomic ratio, *H/Pd,* exists for the entire PdCu alloy compositions range considered here, throughout all the hydrogenation phases (Figures S5 and S6).[16] Using this approach, we also find a linear decrease of *H/Pd* at 250 mbar hydrogen partial pressure for increasing Cu content, in excellent agreement with the bulk system[50] (Figure S7). These results thus validate the use of an optical parameter such as $\Delta\lambda_{peak}$ as direct descriptor of the hydrogen concentration in PdCu alloy nanoparticles, as well as further corroborate homogeneous alloy formation.

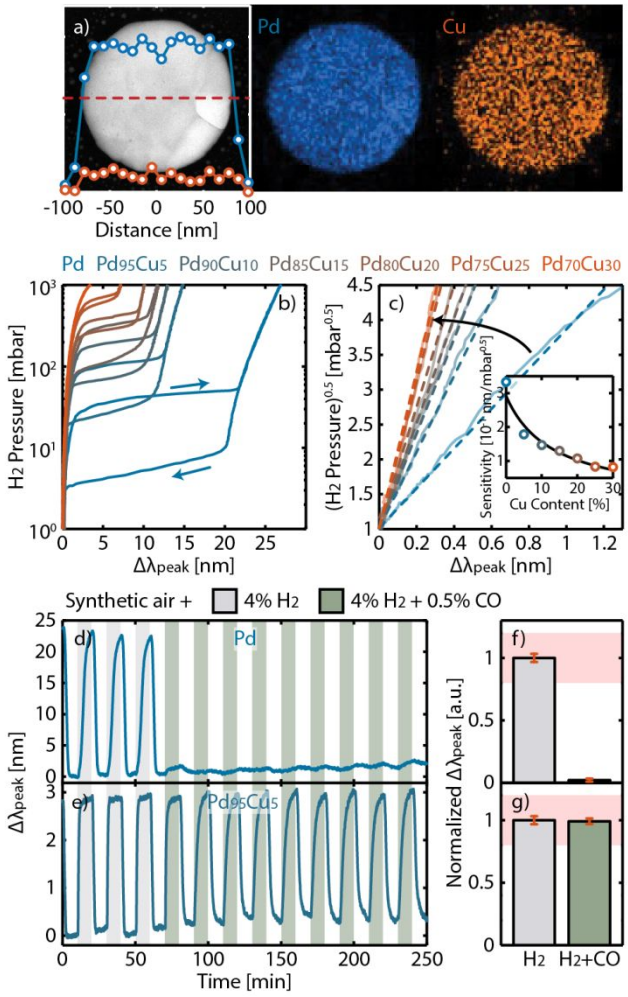

Figure 1. *(a) Left panel: STEM image of a single* $Pd_{85}Cu_{15}$ *nanodisk together with EDS elemental linescans along the corresponding red dashed-line. Right panel: Pd and Cu elemental maps of the nanodisk showing the homogeneity of the alloy throughout the entire particle. (b) PdCu alloy nanoparticle array optical isotherms in the 1–1000 mbar range. The right- and left-pointing arrows denote the hydrogen absorption and desorption branches, respectively. (c)* $\Delta\lambda_{peak}$ *response in the low 1–20 mbar mbar pressure range, plotted as function of square root of hydrogen pressure. A linear correlation between* $\Delta\lambda_{peak}$ *and the square root of hydrogen pressure exists, in good agreement with Sievert's law for a solid solution (dashed lines), and an up to 4 times reduced sensitivity for the PdCu alloy compared to neat Pd is observed as the Cu content*

in the alloy is increased (inset). The arrow points to alloys with higher Cu concentration. Time-dependent $\Delta\lambda_{peak}$ response of (d) Pd and (e) $Pd_{95}Cu_5$ to three 10-min 4% H_2 pulses (grey shaded areas) followed by 9 pulses of 4% H_2 + 0.5% CO mixture (green shaded areas) measured at atmospheric pressure. $\Delta\lambda_{peak}$ response in CO background normalized to the one obtained in pure 4% H_2 for (f) Pd and (g) $Pd_{95}Cu_5$. The error bars denote the standard deviation from 10 cycles. The red shaded areas indicate the ±20% deviation limit from the normalized $\Delta\lambda_{peak}$ in pure 4% H_2 according to the performance standard for hydrogen sensors.[51] *All sensing experiments were carried out at 30 °C.*

We now turn to the analysis of the hydrogen sorption characteristics of the PdCu alloy nanoparticle system. **Figure 1**b shows the hydrogen absorption and desorption isotherms between 1–1000 mbar H_2 for different alloy compositions measured optically in transmission configuration (see Figure S8 for raw optical data) at 30 °C in a vacuum chamber. For pure Pd, the characteristic α-phase region at low-hydrogen pressure where hydrogen is diluted at low concentration in a solid solution; the α + β-phase-coexistence region (**"**plateau**"**) at the first-order phase transition to and from the hydride (β-phase) with wide hysteresis; and finally, the pure β-phase region at high-hydrogen pressure are observed.[52,53] As the Cu content in the alloy increases, the plateau becomes narrower and shifts towards higher hydrogen pressure. Simultaneously, the hysteresis width reduces and hysteresis completely disappears for the case of $Pd_{70}Cu_{30}$.

Increasing the Cu content, however, also reduces the overall absolute value of $\Delta\lambda_{peak}$ for a given hydrogen pressure, which translates to a reduced sensitivity of a sensor based on these systems.

Furthermore, also in the α–phase region at low hydrogen pressure, H solubility is reduced for increasing Cu content (**Figure 1**c) in agreement with the bulk[54,55] but in contrast to the PdAu alloy system where it is found to increase.[11] This lower H-solubility in PdCu alloys stems from repulsive Cu-H pair interactions, as well as from the Pd host lattice contraction induced by addition of Cu due to its smaller atomic radius (*i.e.* α_{Pd} = 3.89 Å, α_{Cu} = 3.61 Å).[54] Consequently, for the hysteresis-free $Pd_{70}Cu_{30}$ system, the sensitivity in the α–phase is reduced by a factor of 4 compared to pure Pd (*i.e.* 0.34 nm/mbar$^{0.5}$ compared to 0.08 nm/mbar$^{0.5}$ – inset **Figure 1**c).

To examine the PdCu alloy sensor response in poisoning conditions, we compared pure Pd and $Pd_{95}Cu_5$ sensors in a high CO background of 0.5% in an atmospheric pressure gas flow system using synthetic air as the carrier gas to determine the minimum amount of Cu required to eliminate CO poisoning. Specifically, we performed these experiments by alternatively exposing the sensors to 10-min pulses of mixed 4% H_2 + 0.5% CO in synthetic air and pure synthetic air. As a control, the samples were initially also exposed to 10 cycles of 4% H_2 in synthetic air and pure synthetic air, respectively. **Figure 1**d and e summarizes the corresponding time-resolved $\Delta\lambda_{peak}$ response for the two considered sensors. Clearly, severe CO poisoning occurs for the pure Pd sample, as apparent from the drastically reduced total $\Delta\lambda_{peak}$ response.[34,35] Remarkably, however, the $Pd_{95}Cu_5$ alloy sensor is only slightly affected by the CO background, demonstrating that adding as little as 5 *at*.% Cu to the alloy is sufficient to prevent CO poisoning and sensor deactivation (see also Figure S9 for results on $Pd_{70}Cu_{30}$ sensor). This is in line with surface science studies of PdCu alloys, which have shown that CO is less strongly bonded to the Pd atoms of the PdCu alloy than to those of neat Pd.[43,56]

To further quantify this key observation, in **Figure 1**f and g we plot the $\Delta\lambda_{peak}$ response in CO background normalized to the one obtained in only H_2. It becomes clear that the $Pd_{95}Cu_5$ alloy sensor essentially preserves its response within ±20% reference signal, *i.e.* the set performance standard for a hydrogen sensor,[51] whereas the Pd sensor response is reduced to less than 5% of the original one.

Drawing some intermediate conclusions to assess the hydrogen sensing performance of the PdCu alloy nanoparticle system, it is clear that it indeed provides resistance towards CO poisoning already at a low Cu content of only 5 *at*.% and thus very likely also for sulfur species.[57,58] However, its main drawback is the significantly reduced sensitivity in the hysteresis free regime for which high Cu content is required, in particular in the low hydrogen pressure regime below the flammability limit of 40 mbar H_2 in air.

One of the central ideas with alloying different elements is to, ideally, be able to combine their respective desired properties in a single material. To this end, we have recently explored the use of PdAu alloy nanoparticles as plasmonic hydrogen sensors.[11,15,18] This alloy, in particular the champion system $Pd_{75}Au_{25}$, displayed superior sensing metrics compared to the pure Pd analogue in that it features hysteresis-free response, sub-second response time at room temperature and most importantly up to 8 times higher sensitivity than pure Pd in the sub-40 mbar hydrogen pressure regime (in contrast to the PdCu system studied above where the corresponding sensitivity is reduced by a factor 4). However, as literature reports and as we show below also for our specific system, PdAu alloys are not resistant to poisoning and deactivation.[34,35,59]

As a consequence, to combine the best of two worlds in our next step, we nanofabricated the *ternary* $Pd_{70}Au_{25}Cu_5$ alloy to emulate our previous champion system $Pd_{75}Au_{25}$, while adding the smallest amount of Cu found above to be required to prevent CO poisoning. To characterize this ternary alloy, we again performed STEM-EDS analysis, which reveals homogeneous alloy formation (**Figure 2**a). As first sensing performance characterization step, we measured the hydrogen absorption and desorption isotherm at 30 °C for $Pd_{70}Au_{25}Cu_5$ together with $Pd_{70}Cu_{30}$ for comparison (**Figure 2**b). It is clear that the hysteresis-free response, as well as the high sensitivity in the low pressure regime, the characteristic of $Pd_{75}Au_{25}$ system,[11] is preserved despite the addition of 5 *at*.% Cu. Moreover, $Pd_{70}Au_{25}Cu_5$ exhibits a consistently higher $\Delta\lambda_{peak}$ response (*i.e.* higher sensitivity) than $Pd_{70}Cu_{30}$ throughout the entire investigated hydrogen pressure range (**Figure 2**c). In particular for the sub-40 mbar regime, the sensitivity of the ternary alloy is nearly an order of magnitude higher.

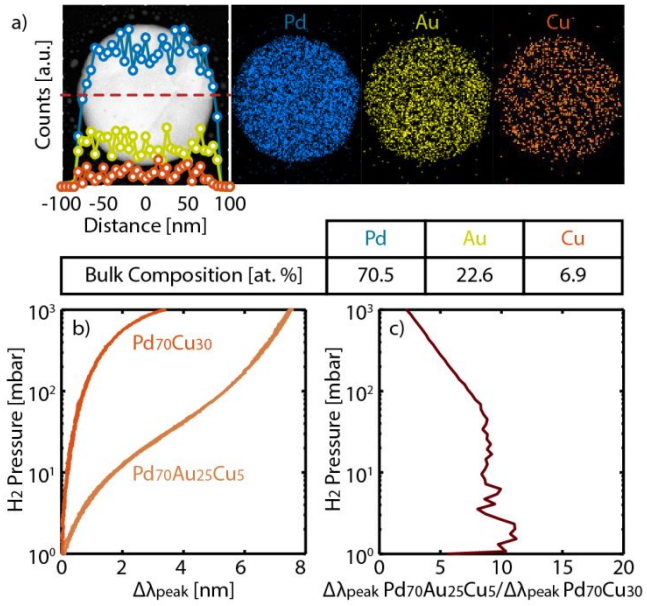

Figure 2. *(a) Top-left: STEM image of a single $Pd_{70}Au_{25}Cu_5$ nanodisk together with EDS elemental line-scans along the corresponding red dashed-line. Top-right: EDS elemental maps of the nanodisk corroborating the homogeneous nature of the alloy. Bottom: Table containing the elemental composition of the $Pd_{70}Au_{25}Cu_5$ alloy nanoparticle, as derived from the EDS analysis. The obtained numbers agree well with the nominal composition within the accuracy of the analysis. (b) Optical absorption and desorption isotherms for the ternary $Pd_{70}Au_{25}Cu_5$ system plotted together with the binary $Pd_{70}Cu_{30}$ system for comparison. Both feature completely hysteresis-free response but the absolute $\Delta\lambda_{peak}$ (i.e. the sensitivity) is significantly higher for the ternary alloy, in particular in the sub-40 mbar pressure range. The up- and downward arrows denote the hydrogen absorption and desorption branches, respectively. (c) Sensitivity enhancement for the ternary system compared to the binary one plotted over 4 orders of hydrogen pressure and expressed as [$\Delta\lambda_{peak}$ ternary alloy/$\Delta\lambda_{peak}$ binary alloy].*

The temporal response of the ternary $Pd_{70}Au_{25}Cu_5$ alloy system during hydrogen sorption to and from 40 mbar at 30 °C, together with the corresponding data for the pure Pd system, are plotted in **Figure 3**. Clearly, for both absorption and desorption, the ternary alloy is faster than the Pd benchmark by an order of magnitude. In fact, the measured response time of 0.4 s at 40 mbar is amongst the fastest optical hydrogen sensors ever reported at these conditions.[11,19,60–62] The origin of this accelerating effect in PdAu alloys has recently been uncovered and is due to the reduction of the apparent activation energy for the hydrogen sorption at the surface upon alloying with Au.[19,63] In our particular case, we empirically find that the addition of 5 *at*.% Cu does not notably influence this effect and thus the fast kinetics are preserved.

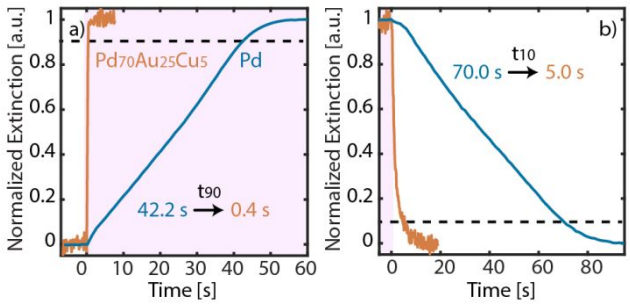

Figure 3. *(a) Absorption and (b) desorption kinetics of a $Pd_{75}Au_{25}Cu_5$ sensor measured in a vacuum chamber by exposing the sample to/from 40 mbar H_2 pressure pulses plotted together with corresponding data for a neat Pd reference. A record response time of 0.4 s is achieved for the ternary $Pd_{75}Au_{25}Cu_5$ alloy. The dashed lines mark the 90% and 10% level of the maximum response, respectively. The red-shaded areas denote 40 mbar H_2 pulses. All experiments were carried out at 30 °C.*

To determine the absolute limit of detection (LoD) of the ternary alloy sensor we first measured the $\Delta\lambda_{peak}$ response in vacuum/pure H_2 at a 1 Hz sampling frequency to be able to resolve the target of 1 s response time[64] for a series of hydrogen pulses in the pressure range from 1 mbar and below (**Figure 4**a). This analysis reveals a remarkable sensitivity of the ternary alloy, as a $\Delta\lambda_{peak}$ response is clearly resolved even at the lowest hydrogen concentration of 10 µbar attainable in our setup in a controlled way, hinting at an even lower LoD. In fact, by defining the LoD as 3σ, where σ denotes the noise of the acquired signal (*i.e.* 0.01 nm,[19,65] *cf.* inset in **Figure 4**a and also Figure S10), we can extrapolate a detection limit in the range of 1–5 µbar (**Figure 4**b). To further assess the sensitivity of the sensor in more realistic conditions, we also conducted similar experiments in Ar and synthetic air carrier gas at atmospheric pressure. In Ar, down to the lowest H_2 concentration attainable in our setup, *i.e.* 10 ppm, a $\Delta\lambda_{peak}$ response similar to what we measured in vacuum is observed (Figure S11). This translates to a detection limit of about 5 ppm. In synthetic air, however, the sensor exhibits smaller $\Delta\lambda_{peak}$ response for a given H_2 concentration (Figure S12) due to the competing processes of the hydrogen oxidation reaction and O blocking the adsorption sites.[66] This results in an extrapolated detection limit in the range of 40–50 ppm. The attained sensitivity in both Ar and air is remarkable as it (i) puts our sensor amongst the most sensitive hydrogen sensors measured in the respective carrier gas,[17,67–69] and (ii) because there is significant further improvement potential by engineering sensitivity, following our design rule of red-shifting the LSPR by tailoring particle geometry.[16]

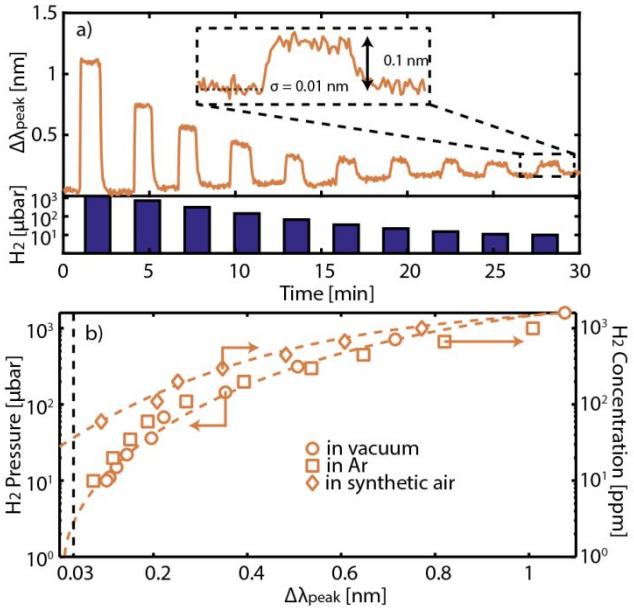

Figure 4. *(a) $\Delta\lambda_{peak}$ response for a series of hydrogen pulses in the pressure range from 1 mbar down to 10 μbar for $Pd_{70}Au_{25}Cu_5$, measured in a vacuum chamber. Note the clear response even at 10 μbar (the lowest pressure attainable in our setup in a controlled way), shown in the inset. The integration time for the data was 1 Hz and the typical noise is σ = 0.01 nm. (b) $\Delta\lambda_{peak}$ response of the $Pd_{70}Au_{25}Cu_5$ sensor measured in vacuum/pure H_2 (circles), Ar carrier gas (squares) and synthetic air carrier gas (diamonds) as function of the H_2 pressure for the former and H_2 concentration in ppm for the latter two. By defining the limit of detection (LoD) as 3σ = 0.03 nm, marked by the dashed line, we can extrapolate the LoD to the range between 1–5 ppm and 40–50 ppm for the ternary alloy sensor in Ar and synthetic air, respectively. All experiments were carried out at 30 °C.*

To assess the resistance of the ternary $Pd_{70}Au_{25}Cu_5$ alloy towards CO poisoning, we employed the same experimental protocol as used above for the binary system using synthetic air as the

carrier gas. In addition, we also investigated the impact of CO_2 and CH_4 on the system. For the $Pd_{75}Au_{25}$ binary control, severe sensor poisoning occurs in CO background as expected[34] (**Figure 5**a), and the signal amplitude degrades to about 35% of the reference signal in the absence of CO after 10 cycles (**Figure 5**c). However, for the ternary $Pd_{70}Au_{25}Cu_5$ alloy, no sensor poisoning occurs (**Figure 5**b) and the maximum $\Delta\lambda_{peak}$ signal amplitude at 4% H_2 in synthetic air carrier gas is maintained also in 0.5% CO background and lies well within the ±20% deviation limit performance standard for hydrogen sensors (**Figure 5**d).[51] This is further corroborated by an extended test of over 50 hydrogen cycles in *constant* synthetic air + 0.5% CO background, for which no sensor degradation or deactivation occurs (**Figure 5**e). To this end, we note that the resistance towards CO also persists for exposure to lower hydrogen concentrations (*i.e.* 1% and 0.1%, see Figures S13 and S14, respectively), however with decelerating response time, which is proportional to the CO/H_2 abundance and thus hints at reaction between H_2 and CO to form hydrocarbons even at the present mild conditions. Finally, we also tested the influence of CO_2 and CH_4 on sensor performance and found that neither 2% CO_2 nor 0.5% CH_4 in the gas feed affect the ternary alloy system (Figure S15).

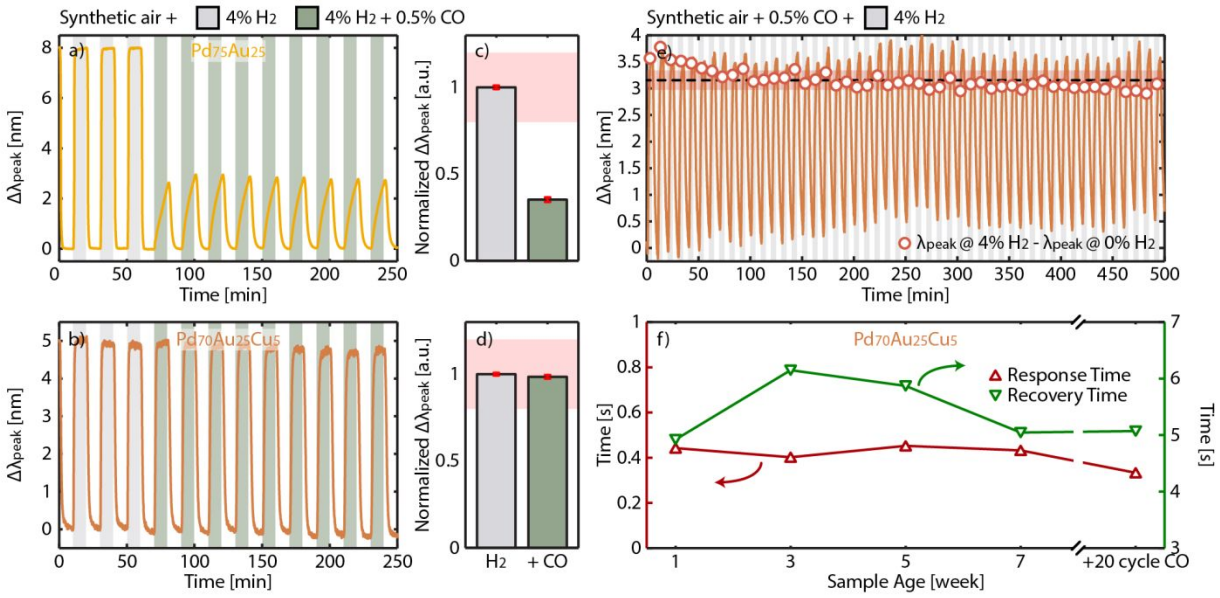

Figure 5. *Time-resolved $\Delta\lambda_{peak}$ response of (a) binary alloy $Pd_{75}Au_{25}$ control and (b) the ternary alloy $Pd_{70}Au_{25}Cu_5$ to three 4% H_2 pulses (grey shaded areas) followed by 9 pulses of 4% H_2 + 0.5% CO (green shaded areas), both in synthetic air carrier gas. $\Delta\lambda_{peak}$ response in CO background normalized to the one obtained in pure 4% H_2 for (c) $Pd_{75}Au_{25}$ and (d) $Pd_{70}Au_{25}Cu_5$. The error bars denote the standard deviation from 10 cycles. The red shaded areas indicate the ±20% deviation limit from the normalized $\Delta\lambda_{peak}$ in pure 4% H_2 according to the performance standard for hydrogen sensors.*[51] *(e) Time-resolved $\Delta\lambda_{peak}$ response of $Pd_{70}Au_{25}Cu_5$ ternary alloy sensor to 50 cycles of 4% H_2 in a constant 0.5% CO background in synthetic air. The sensor exhibit excellent CO-resistant throughout the measurement as indicated by constant $\Delta\lambda_{peak}$ signal amplitude (circles). The dashed line and red shaded area mark the mean and standard deviation of the $\Delta\lambda_{peak}$ signal amplitude from the corresponding 50 cycles, respectively. (f) Response and recovery times of $Pd_{70}Au_{25}Cu_5$ alloy at different conditions, which show maintained 0.4 s and 5 s response and recovery time, respectively, throughout the entire 7-week period, as well as after exposure to severe CO poisoning conditions. All experiments were carried out at 30 °C.*

As the final assessment, we investigated the long-term stability of our ternary system. This is motivated by the lifetime requirement of practical hydrogen sensors, and due to the fact that alloyant segregation to the surface occurs in alloys,[70] which, specifically for our case, may influence the hydrogen sorption kinetics and thermodynamics.[25,26,71] To do so, we casually placed the $Pd_{70}Au_{25}Cu_5$ alloy sample on a lab bench over a 7-week period and continuously characterized its surface composition by X-ray Photoelectron Spectroscopy (XPS), as well as repeatedly measured its key hydrogen sensing metrics. XPS analysis reveals that the alloy exhibits remarkably constant surface composition over time, *i.e.* no further segregation occurs after fabrication (Figure S16). This is in line with the reported low segregation energy of Cu.[72,73] Furthermore, no sign of Cu oxide formation is found in XPS due the complete absence of a characteristic CuO peak at 940 eV (Figure S17). This excellent surface stability is also reflected in the unchanged thermodynamic and kinetic response of the alloy to hydrogen over time (Figure S18). Specifically, the response and recovery times of around 0.4 s and 5 s, respectively, remain unchanged even after 7 weeks and even after exposure to CO poisoning environment (**Figures 5**f and S19).

Having above rigorously assessed the ternary alloy sensor performance, it is important to put the obtained sensing metrics in a wider perspective. To this end, given the diverse application areas of hydrogen sensors, key stakeholders have formulated explicit guidelines and performance targets for hydrogen sensors, with different requirements depending on the application.[64,74] The most stringent requirements to date have been set for hydrogen sensors to be used in safety systems and they were formulated by the U.S. Department of Energy, DoE (**Table 1**). For example, in such an

application the sensor must respond within one second when exposed to 4 *vol*. % H_2, the lower flammability limit of a hydrogen-air mixture. In **Table 1**, we summarize the key sensing parameters of our sensor based on the $Pd_{70}Au_{25}Cu_5$ material together with the other CO-resistant sensors reported in the literature. We find that our system exhibits superior performance and meets the set DoE targets. Furthermore, expanding the performance comparison of our $Pd_{70}Au_{25}Cu_5$ solution to hydrogen sensors *in general* reported in the literature (*i.e.* including also sensors for which CO-resistance has *not* been explicitly assessed), places it amongst the best sensors with respect to response time and LoD, even when including the family of technically more mature electrical sensors (Table S2).

Table 1. Technical performance requirements for hydrogen sensors for safety systems and sensing metrics of CO-resistant hydrogen sensors from the literature.

Parameter	Safety Systems Requirements [75,76]	Sensor Platform				
		Pd NP[a]/graphene @ PMMA[40]	Pd NP[a] @ PMMA[41]	Pd film @ HKUST-1[42]	PdAu @ PTFE @ PMMA[19]	PdAuCu NP[a] (this work)
Measurement Range	0.1 - 10%	0.025 - 2%	10%	Up to 100%	1 ppm – 100%	5 ppm – 100%
Detection Limit	1000 ppm	250 ppm	50 ppm	n.a.	1 ppm	5 ppm
Operating Temperature	-30 – 80 °C	RT[b]	RT[b]	100 °C[b]	30 °C[b]	30 °C[b]
Response	< 1 s	108 s[c]	11 s[d]	170 s[c]	0.3 s[d]	0.4 s[d]

Time						
Recovery Time	< 60 s	330 s[c]	n.a.	n.a.	4 s[d]	5 s[d]
Uncertainty	< 5%	n.a.	n.a.	Hysteresis	Hysteresis-free	Hysteresis-free

n.a. = not addressed. [a]NP = nanoparticles. [b]Temperature at response/recovery time measurements. RT = room temperature. [c]Response to/from 2% H_2. [d]Response to/from 4% H_2.

In summary, we have shown that already a Cu content as low as 5 *at*.% in binary PdCu alloy nanoparticles provides a very high resistance towards CO poisoning and effectively prevents deactivation in CO background in synthetic air, a condition which immediately deactivates the neat Pd control, when used as optical hydrogen sensors. Furthermore, hysteresis in the optical response to applied hydrogen partial pressure can be engineered and completely eliminated at a 30 *at*.% Cu content in the alloy. However, this comes at the price of a decreased overall sensitivity of the PdCu alloy sensors due to the linearly decreasing amount of hydrogen absorbed at a given hydrogen partial pressure for increasing Cu content in the alloy, and the concurrently reduced absolute sensor response. To ameliorate this limiting factor, we demonstrated that *combining* a multitude of beneficial effects characteristic to alloying Pd with the coinage metals Cu and Au in their respective binary alloys in a combined *ternary* system, enables the rational design of nanoplasmonic hydrogen sensors with unprecedented sensing metrics. Specifically, by exploiting synergistic effects between the CO-poisoning resistant PdCu alloy system, and the highly hydrogen sensitive PdAu alloy system, we introduced a $Pd_{70}Au_{25}Cu_5$ ternary alloy plasmonic hydrogen sensor which displays: (i) detection limit in the ppm range, (ii) hysteresis-free response over 5 orders of magnitude hydrogen pressure, (iii) sub-second response time at room temperature, (iv) CO, CO_2 and CH_4 poisoning resistance in synthetic air and (v) excellent

stability over time, altogether meeting or even exceeding the corresponding strict hydrogen sensor performance targets [64,75,76]. Notably, these metrics are achieved without applying any protective coatings, such as polymers or metal organic frameworks [19,40–42,77,78] and it is very likely that our approach facilitates a similarly high resistance to deactivation by sulfuric species, based on the related literature[57,58].

In a wider perspective, our work opens the door to next-generation plasmonic hydrogen gas sensors based on rational materials design centered on the idea of combining beneficial traits of binary alloys in more complex material systems, to enable the optimization of deactivation resistance, response time, selectivity and limit of detection and thus meet the ever increasing demand for advanced sensor technologies. Furthermore, we predict that the developed binary and ternary alloy nanoparticles will find application in other areas of nanoplasmonics where the alloying concept provides an alternative handle to tailor optical properties,[15,79,80] and in heterogeneous catalysis where the developed structures may serve as model systems for systematic investigations of alloying impact on catalyst activity and selectivity.

Methods

Sample Fabrication. PdCu alloy nanodisk arrays were fabricated using layer-by-layer deposition through a hole-mask[48] onto 1×1 cm glass substrates (Borofloat, Schott Scandinavia AB), on TEM windows (for EDS elemental mapping), on oxidized silicon wafer substrates (for SEM

imaging), and on QCM crystals (Laptech, SC-cut, 10 MHz fundamental frequency). Deposition was followed by annealing at 500 ^{o}C for 24 h under flow of 4% H_2 in Ar.[15] A more detailed description of the nanofabrication procedure can be found in our earlier work.[15] For the QCM crystals, prior to the fabrication of the alloy nanoparticles, a 1 nm Cr adhesion layer and 100 nm SiO_2 were deposited using a Lesker 225 e-beam PVD system (rate 1 Å/s, base pressure 5×10^{-7} Torr) and an STS PECVD system, respectively. This is necessary to avoid coupling between LSPR in the nanoparticles and the Au electrode of the QCM crystal via image charge effects. It is also worth noting that for the QCM sensor, annealing was done at 400 °C for 72 h (lower temperature and longer time than in the standard method however yielding the same result) to avoid α-β phase transformation in quartz at 450 °C that leads to cracking.

Nanoparticle and Alloy Characterization. Several different characterization techniques were used, namely scanning electron microscopy (SEM), scanning transmission electron microscopy (STEM), energy dispersive X-ray spectroscopy (EDS) and X-ray photoelectron spectroscopy (XPS). All SEM images were obtained in a Zeiss Supra 60 VP with secondary electron detector, working distance 4 mm, and electron beam acceleration voltage of 10–15 kV. STEM – EDS measurements were taken using an FEI Titan TEM instrument operated at 300 kV acceleration voltage. The electron probe diameter and convergence semi-angle were approximately 0.15 nm and 17.5 mrad, respectively. HAADF STEM images were recorded with a collection semi-angle of approximately 47 mrad. EDS maps were obtained with a pixel size of ~5 nm and acquisition time of 1 s per pixel. The EDS maps were analyzed in Aztec 3.3 (Oxford Instruments). XPS measurements were carried out with a PerkinElmer PHI 5000C ESCA system. The scanning resolution is 0.125 eV. The C peak was set to 384.5 eV and used as reference. The atomic

composition was calculated using the MultiPak 6.0 software, which employs a Shirley-type background correction.

Hydrogenation Isotherm, Kinetics and Sensitivity Measurements. The binary PdCu and ternary PdAuCu alloy isotherm, kinetics and sensitivity measurements in pure H_2 were performed in a custom-made vacuum chamber setup with optical windows reported earlier.[11,15] The absolute hydrogen pressure in the chamber was monitored using two capacitive pressure gauges with different range (MKS Baratron). Optical transmittance through the sample was enabled by UHV-compatible sapphire windows mounted on the vacuum chamber, and by using a fiber-coupled, unpolarized white light source (Avantes AvaLight-Hal) and a fixed grating fiber coupled spectrophotometer (Avantes SensLine AvaSpec-2048XL). The pressure inside the chamber was controlled using a microbar-precision leak valve. The temperature was controlled with a heating coil wrapped around the chamber and a temperature controller (Eurotherm 3216N) in a feedback loop manner, where the sample surface temperature inside the vacuum chamber was continuously used as input. We performed all of our experiments at constant 30 °C. The kinetics measurements were performed at 6 Hz frequency (0.165 ms integration time with 10 averages). The isotherm and sensitivity measurements were performed at 1 Hz sampling frequency (0.165 ms integration time with 1000 averages). It is important to note that the apparent sampling frequency obtained by the setup is slower than the theoretical one (*i.e.* integration time × averaging number) due to the delay in the computing system when acquiring, processing, analyzing and plotting the data in real time. The LSPR peak descriptors were obtained by fitting a Lorentzian to the wavelength range

at at ±60 nm around the LSPR peak in the measured optical extinction spectra, which gives good fit ($R^2 > 0.96$) despite the asymmetry in the broad LSPR peak (Figure S10).[19]

Deactivation Tests and Sensitivity Measurements in Ar and Synthetic Air. The deactivation and sensitivity measurements in Ar and synthetic air measurements were carried out in quartz tube flow reactor at atmospheric pressure with optical access for transmittance measurements (X1, Insplorion AB), using synthetic air as the carrier gas.[81] The gas flow rate (kept constant at 100 mL/min, 500 mL/min and 325 mL/min for deactivation and sensitivity measurements in Ar and synthetic air, respectively) and gas composition were controlled by mass flow controllers (Bronkhorst ΔP). The sample inside the flow reactor was illuminated by white light (AvaLight-Hal, Avantes) through an optical fiber equipped with a collimating lens. The transmitted light was then analyzed using a fiber-coupled fixed-grating spectrometer (AvaSpec-1024, Avantes or SensLine AvaSpec-2048XL, Avantes, for sensitivity measurements). The measurement temperature was kept at 30 °C.

Simultaneous QCM and LSPR Measurements: The QCM window-module (QSense Explorer Microscopy, Biolin Scientific Corporation) was connected to a series of mass flow controllers (Bronkhorst ΔP) to regulate the H_2 partial pressure in Ar carrier gas at a constant total flow rate of 30 mL/min. A bifurcated fiber optic reflectance probe (FCR-7UV400C-2-ME-HTX, Avantes) positioned above the window was connected to a light source (AvaLight-Hal-S, Avantes) and a fixed-grating spectrophotometer (AvaSpec HS-TEC, Avantes). Data collection for QCM and LSPR measurements was executed by

QTools® (Biolin Scientific AB) and Insplorer® (Insplorion AB) softwares, respectively. The absorbed hydrogen content in the nanoparticles was calculated from the quartz crystal resonance frequency shift *via* the Sauerbrey equation[82] and analysis of the nanoparticle surface coverage based on SEM images of the crystal, as described in detail in the Supplementary Information. All of the measurement were carried out at 30 °C.

ASSOCIATED CONTENT

Supporting Information

Electron microscopy images and elemental maps of PdCu alloys, optical properties of PdCu alloy nanoparticles with different composition, simultaneous plasmonic and quartz crystal microbalance measurements, extinction spectra upon hydrogen sorption, $Pd_{70}Cu_{30}$ deactivation test, determination of experimental λ_{peak} and noise, $\Delta\lambda_{peak}$ response in low hydrogen concentration, $Pd_{70}Au_{25}Cu_5$ alloy nanoparticles resistance towards CO at lower H_2 pressure, $Pd_{70}Au_{25}Cu_5$ alloy nanoparticles resistance towards CO_2 and CH_4, $Pd_{70}Au_{25}Cu_5$ alloy nanoparticles stability over time, sensing metrics of state-of-the-art hydrogen sensors from the literature. This material is available free of charge *via* the Internet at http://pubs.acs.org.

AUTHOR INFORMATION

Corresponding Author

*clangham@chalmers.se

Author Contributions

The manuscript was written through contributions of all authors. All authors have given approval to the final version of the manuscript. ‡These authors contributed equally.

Notes

CL is co-founder of a company that markets nanoplasmonic sensors. All other authors declare no competing financial interest.

ACKNOWLEDGMENTS

We acknowledge financial support from the Swedish Foundation for Strategic Research Framework project RMA15-0052 and the Knut and Alice Wallenberg Foundation project 2016.0210. We also thank the Knut and Alice Wallenberg Foundation for their support of the infrastructure in the MC2 nanofabrication laboratory at Chalmers.

REFERENCES

(1) Hydrogen to the Rescue. *Nature Materials*, 2018, *17*, 565.

(2) Schlapbach, L. Technology: Hydrogen-Fuelled Vehicles. *Nature* **2009**, *460*, 809–811.

(3) Buttner, W. J.; Post, M. B.; Burgess, R.; Rivkin, C. An Overview of Hydrogen Safety Sensors and Requirements. *Int. J. Hydrogen Energy* **2011**, *36*, 2462–2470.

(4) Rana, S. V.; Malik, A. Hydrogen Breath Tests in Gastrointestinal Diseases. *Indian J. Clin. Biochem.* **2014**, *29*, 398–405.

(5) Zhao, D.; Wang, T.; Heineman, W. R. Advances in H2 Sensors for Bioanalytical Applications. *TrAC - Trends Anal. Chem.* **2016**, *79*, 269–275.

(6) Bakenne, A.; Nuttall, W.; Kazantzis, N. Sankey-Diagram-Based Insights into the Hydrogen Economy of Today. *Int. J. Hydrogen Energy* **2016**, *41*, 7744–7753.

(7) Hübert, T.; Boon-Brett, L.; Black, G.; Banach, U. Hydrogen Sensors - A Review. *Sensors Actuators, B Chem.* **2011**, *157*, 329–352.

(8) Palmisano, V.; Weidner, E.; Boon-Brett, L.; Bonato, C.; Harskamp, F.; Moretto, P.; Post, M. B.; Burgess, R.; Rivkin, C.; Buttner, W. J. Selectivity and Resistance to Poisons of Commercial Hydrogen Sensors. *Int. J. Hydrogen Energy* **2015**, *40*, 11740–11747.

(9) El Matbouly, H.; Domingue, F.; Palmisano, V.; Boon-Brett, L.; Post, M. B.; Rivkin, C.; Burgess, R.; Buttner, W. J. Assessment of Commercial Micro-Machined Hydrogen Sensors Performance Metrics for Safety Sensing Applications. *Int. J. Hydrogen Energy* **2014**, *39*, 4664–4673.

(10) Wadell, C.; Syrenova, S.; Langhammer, C. Plasmonic Hydrogen Sensing with Nanostructured Metal Hydrides. *ACS Nano* **2014**, *8*, 11925–11940.

(11) Wadell, C.; Nugroho, F. A. A.; Lidström, E.; Iandolo, B.; Wagner, J. B.; Langhammer, C. Hysteresis-Free Nanoplasmonic Pd-Au Alloy Hydrogen Sensors. *Nano Lett.* **2015**, *15*, 3563–3570.

(12) Yip, H. K.; Zhu, X.; Zhuo, X.; Jiang, R.; Yang, Z.; Wang, J. Gold Nanobipyramid-Enhanced Hydrogen Sensing with Plasmon Red Shifts Reaching ≈140 Nm at 2 Vol% Hydrogen Concentration. *Adv. Opt. Mater.* **2017**, *5*, 1700740.

(13) Liu, N.; Tang, M. L.; Hentschel, M.; Giessen, H.; Alivisatos, A. P. Nanoantenna-Enhanced Gas Sensing in a Single Tailored Nanofocus. *Nat. Mater.* **2011**, *10*, 631–636.

(14) Matuschek, M.; Singh, D. P.; Jeong, H. H.; Nesterov, M.; Weiss, T.; Fischer, P.; Neubrech, F.; Liu, N. Chiral Plasmonic Hydrogen Sensors. *Small* **2018**, *14*, 1702990.

(15) Nugroho, F. A. A.; Iandolo, B.; Wagner, J. B.; Langhammer, C. Bottom-Up Nanofabrication of Supported Noble Metal Alloy Nanoparticle Arrays for Plasmonics. *ACS Nano* **2016**, *10*, 2871–2879.

(16) Nugroho, F. A. A.; Darmadi, I.; Zhdanov, V. P.; Langhammer, C. Universal Scaling and Design Rules of Hydrogen-Induced Optical Properties in Pd and Pd-Alloy Nanoparticles. *ACS Nano* **2018**, *12*, 9903–9912.

(17) He, J.; Villa, N. S.; Luo, Z.; An, S.; Shen, Q.; Tao, P.; Song, C.; Wu, J.; Deng, T.; Shang, W. Integrating Plasmonic Nanostructures with Natural Photonic Architectures in Pd-Modified *Morpho* Butterfly Wings for Sensitive Hydrogen Gas Sensing. *RSC Adv.* **2018**, *8*, 32395–32400.

(18) Nugroho, F. A. A.; Eklund, R.; Nilsson, S.; Langhammer, C. A Fiber-Optic Nanoplasmonic Hydrogen Sensor via Pattern-Transfer of Nanofabricated PdAu Alloy Nanostructures. *Nanoscale* **2018**, *10*, 20533–20539.

(19) Nugroho, F. A. A.; Darmadi, I.; Cusinato, L.; Susarrey-Arce, A.; Schreuders, H.; Bannenberg, L. J.; da Silva Fanta, A. B.; Kadkhodazadeh, S.; Wagner, J. B.; Antosiewicz, T. J.; *et al.* Metal–Polymer Hybrid Nanomaterials for Plasmonic Ultrafast Hydrogen Detection. *Nat. Mater.* **2019**, *18*, 489–495.

(20) Langhammer, C.; Zorić, I.; Kasemo, B.; Clemens, B. M. Hydrogen Storage in Pd Nanodisks Characterized with a Novel Nanoplasmonic Sensing Scheme. *Nano Lett.* **2007**, *7*, 3122–3127.

(21) Sterl, F.; Strohfeldt, N.; Walter, R.; Griessen, R.; Tittl, A.; Giessen, H. Magnesium as Novel Material for Active Plasmonics in the Visible Wavelength Range. *Nano Lett.* **2015**, *15*, 7949–7955.

(22) Strohfeldt, N.; Tittl, A.; Schäferling, M.; Neubrech, F.; Kreibig, U.; Griessen, R.; Giessen, H. Yttrium Hydride Nanoantennas for Active Plasmonics. *Nano Lett.* **2014**, *14*, 1140–1147.

(23) Jiang, R.; Qin, F.; Ruan, Q.; Wang, J.; Jin, C. Ultrasensitive Plasmonic Response of Bimetallic Au/Pd Nanostructures to Hydrogen. *Adv. Funct. Mater.* **2014**, *24*, 7328–7337.

(24) Syrenova, S.; Wadell, C.; Nugroho, F. A. A.; Gschneidtner, T. A.; Diaz Fernandez, Y. A.; Nalin, G.; Świtlik, D.; Westerlund, F.; Antosiewicz, T. J.; Zhdanov, V. P.; *et al.* Hydride Formation Thermodynamics and Hysteresis in Individual Pd Nanocrystals with Different

Size and Shape. *Nat. Mater.* **2015**, *14*, 1236–1244.

(25) Baldi, A.; Narayan, T. C.; Koh, A. L.; Dionne, J. A. In Situ Detection of Hydrogen-Induced Phase Transitions in Individual Palladium Nanocrystals. *Nat. Mater.* **2014**, *13*, 1143–1148.

(26) Alekseeva, S.; Fanta, A. B. da S.; Iandolo, B.; Antosiewicz, T. J.; Nugroho, F. A. A.; Wagner, J. B.; Burrows, A.; Zhdanov, V. P.; Langhammer, C. Grain Boundary Mediated Hydriding Phase Transformations in Individual Polycrystalline Metal Nanoparticles. *Nat. Commun.* **2017**, *8*, 1084.

(27) Isaac, N. A.; Ngene, P.; Westerwaal, R. J.; Gaury, J.; Dam, B.; Schmidt-Ott, A.; Biskos, G. Optical Hydrogen Sensing with Nanoparticulate Pd–Au Films Produced by Spark Ablation. *Sensors Actuators B Chem.* **2015**, *221*, 290–296.

(28) Boelsma, C.; Bannenberg, L. J.; van Setten, M. J.; Steinke, N.-J.; van Well, A. A.; Dam, B. Hafnium—an Optical Hydrogen Sensor Spanning Six Orders in Pressure. *Nat. Commun.* **2017**, *8*, 15718.

(29) Adams, B. D.; Chen, A. The Role of Palladium in a Hydrogen Economy. *Mater. Today* **2011**, *14*, 282–289.

(30) Schwarz, R. B.; Khachaturyan, A. G. Thermodynamics of Open Two-Phase Systems with Coherent Interfaces: Application to Metal–hydrogen Systems. *Acta Mater.* **2006**, *54*, 313–323.

(31) Westerwaal, R. J.; Rooijmans, J. S. A.; Leclercq, L.; Gheorghe, D. G.; Radeva, T.; Mooij,

L.; Mak, T.; Polak, L.; Slaman, M.; Dam, B.; *et al.* Nanostructured Pd–Au Based Fiber Optic Sensors for Probing Hydrogen Concentrations in Gas Mixtures. *Int. J. Hydrogen Energy* **2013**, *38*, 4201–4212.

(32) Lee, E.; Lee, J. M.; Lee, E.; Noh, J.-S.; Joe, J. H.; Jung, B.; Lee, W. Hydrogen Gas Sensing Performance of Pd–Ni Alloy Thin Films. *Thin Solid Films* **2010**, *519*, 880–884.

(33) Korotcenkov, G.; Han, S. Do; Stetter, J. R. Review of Electrochemical Hydrogen Sensors. *Chem. Rev.* **2009**, *109*, 1402–1433.

(34) Ogura, S.; Fukutani, K. Dynamic Blocking by CO of Hydrogen Transport across Pd 70 Au 30 (110) Surfaces. *J. Phys. Chem. C* **2017**, *121*, 3373–3380.

(35) Ogura, S.; Okada, M.; Fukutani, K. Near-Surface Accumulation of Hydrogen and CO Blocking Effects on a Pd–Au Alloy. *J. Phys. Chem. C* **2013**, *117*, 9366–9371.

(36) O'Brien, C. P.; Lee, I. C. The Interaction of CO with PdCu Hydrogen Separation Membranes: An Operando Infrared Spectroscopy Study. *Catal. Today* **2017**. DOI: 10.1016/j.cattod.2017.09.039

(37) Jung, S. H.; Kusakabe, K.; Morooka, S.; Kim, S.-D. Effects of Co-Existing Hydrocarbons on Hydrogen Permeation through a Palladium Membrane. *J. Memb. Sci.* **2000**, *170*, 53–60.

(38) Liu, K.; Song, C.; Subramani, V. *Hydrogen and Syngas Production and Purification Technologies*; Liu, K.; Song, C.; Subramani, V., Eds.; John Wiley & Sons, Inc.: Hoboken, NJ, USA, 2009.

(39) Clerbaux, C.; Edwards, D. P.; Deeter, M.; Emmons, L.; Lamarque, J.-F.; Tie, X. X.; Massie, S. T.; Gille, J. Carbon Monoxide Pollution from Cities and Urban Areas Observed by the Terra/MOPITT Mission. *Geophys. Res. Lett.* **2008**, *35*, L03817.

(40) Hong, J.; Lee, S.; Seo, J.; Pyo, S.; Kim, J.; Lee, T. A Highly Sensitive Hydrogen Sensor with Gas Selectivity Using a PMMA Membrane-Coated Pd Nanoparticle/Single-Layer Graphene Hybrid. *ACS Appl. Mater. Interfaces* **2015**, *7*, 3554–3561.

(41) Chen, M.; Mao, P.; Qin, Y.; Wang, J.; Xie, B.; Wang, X.; Han, D.; Wang, G. H.; Song, F.; Han, M.; *et al.* Response Characteristics of Hydrogen Sensors Based on PMMA-Membrane-Coated Palladium Nanoparticle Films. *ACS Appl. Mater. Interfaces* **2017**, *9*, 27193–27201.

(42) Szilágyi, P. Á.; Westerwaal, R. J.; Van De Krol, R.; Geerlings, H.; Dam, B. Metal-Organic Framework Thin Films for Protective Coating of Pd-Based Optical Hydrogen Sensors. *J. Mater. Chem. C* **2013**, *1*, 8146–8155.

(43) Debauge, Y.; Abon, M.; Bertolini, J. C.; Massardier, J.; Rochefort, A. Synergistic Alloying Behaviour of Pd50Cu50 Single Crystals upon Adsorption and Co-Adsorption of CO and NO. *Appl. Surf. Sci.* **1995**, *90*, 15–27.

(44) Rochefort, A.; Fournier, R. Quantum Chemical Study of CO and NO Bonding to Pd2, Cu2, and PdCu. *J. Phys. Chem.* **1996**, *100*, 13506–13513.

(45) Illas, F.; López, N.; Ricart, J. M.; Clotet, A.; Conesa, J. C.; Fernández-García, M. Interaction of CO and NO with PdCu(111) Surfaces. *J. Phys. Chem. B* **1998**, *102*, 8017–8023.

(46) Mak, T.; Westerwaal, R. J.; Slaman, M.; Schreuders, H.; van Vugt, A. W.; Victoria, M.; Boelsma, C.; Dam, B. Optical Fiber Sensor for the Continuous Monitoring of Hydrogen in Oil. *Sensors Actuators B Chem.* **2014**, *190*, 982–989.

(47) Westerwaal, R. J.; den Besten, C.; Slaman, M.; Dam, B.; Nanu, D. E.; Böttger, A. J.; Haije, W. G. High Throughput Screening of Pd-Alloys for H2 Separation Membranes Studied by Hydrogenography and CVM. *Int. J. Hydrogen Energy* **2011**, *36*, 1074–1082.

(48) Fredriksson, H.; Alaverdyan, Y.; Dmitriev, A.; Langhammer, C.; Sutherland, D. S.; Zäch, M.; Kasemo, B. Hole–Mask Colloidal Lithography. *Adv. Mater.* **2007**, *19*, 4297–4302.

(49) Howard, B. .; Killmeyer, R. .; Rothenberger, K. .; Cugini, A. .; Morreale, B. .; Enick, R. .; Bustamante, F. Hydrogen Permeance of Palladium–copper Alloy Membranes over a Wide Range of Temperatures and Pressures. *J. Memb. Sci.* **2004**, *241*, 207–218.

(50) Galipaud, J.; Martin, M. H.; Roué, L.; Guay, D. Pulsed Laser Deposition of PdCuAu Alloy Membranes for Hydrogen Absorption Study. *J. Phys. Chem. C* **2015**, *119*, 26451–26458.

(51) *ISO 26142:2010 Hydrogen Detection Apparatus - Stationary Applications*; 2010.

(52) Zoric´, I.; Larsson, E. M.; Kasemo, B.; Langhammer, C. Localized Surface Plasmons Shed Light on Nanoscale Metal Hydrides. *Adv. Mater.* **2010**, *22*, 4628–4633.

(53) Poyli, M. A.; Silkin, V. M.; Chernov, I. P.; Echenique, P. M.; Muiño, R. D.; Aizpurua, J. Multiscale Theoretical Modeling of Plasmonic Sensing of Hydrogen Uptake in Palladium Nanodisks. *J. Phys. Chem. Lett.* **2012**, *3*, 2556–2561.

(54) Sakamoto, Y.; Ishimaru, N.; Mukai, Y. Thermodynamics of Solution of Hydrogen in Pd-Cu and Pd-Cu-Au Solid Solution Alloys. *Berichte der Bunsengesellschaft für Phys. Chemie* **1991**, *95*, 680–688.

(55) Burch, R.; Buss, R. G. Absorption of Hydrogen by Palladium–copper Alloys. Part 1.—Experimental Measurements. *J. Chem. Soc. Faraday Trans. 1 Phys. Chem. Condens. Phases* **1975**, *71*, 913.

(56) Rochefort, A.; Abon, M.; Delichère, P.; Bertolini, J. C. Alloying Effect on the Adsorption Properties of Pd50Cu50{111} Single Crystal Surface. *Surf. Sci.* **1993**, *294*, 43–52.

(57) Kamakoti, P.; Morreale, B. D.; Ciocco, M. V; Howard, B. H.; Killmeyer, R. P.; Cugini, A. V; Sholl, D. S. Prediction of Hydrogen Flux through Sulfur-Tolerant Binary Alloy Membranes. *Science* **2005**, *307*, 569–573.

(58) Morreale, B. .; Ciocco, M. .; Howard, B. .; Killmeyer, R. .; Cugini, A. .; Enick, R. . Effect of Hydrogen-Sulfide on the Hydrogen Permeance of Palladium–copper Alloys at Elevated Temperatures. *J. Memb. Sci.* **2004**, *241*, 219–224.

(59) Soma-Noto, Y.; Sachtler, W. M. H. Infrared Spectra of Carbon Monoxide Adsorbed on Supported Palladium and Palladium-Silver Alloys. *J. Catal.* **1974**, *32*.

(60) Villatoro, J.; Monzón-Hernández, D. Fast Detection of Hydrogen with Nano Fiber Tapers Coated with Ultra Thin Palladium Layers. *Opt. Express* **2005**, *13*, 5087.

(61) Perrotton, C.; Westerwaal, R. J.; Javahiraly, N.; Slaman, M.; Schreuders, H.; Dam, B.; Meyrueis, P. A Reliable, Sensitive and Fast Optical Fiber Hydrogen Sensor Based on

Surface Plasmon Resonance. *Opt. Express* **2013**, *21*, 382.

(62) Monzón-Hernández, D.; Luna-Moreno, D.; Martínez-Escobar, D. Fast Response Fiber Optic Hydrogen Sensor Based on Palladium and Gold Nano-Layers. *Sensors Actuators B Chem.* **2009**, *136*, 562–566.

(63) Namba, K.; Ogura, S.; Ohno, S.; Di, W.; Kato, K.; Wilde, M.; Pletikosić, I.; Pervan, P.; Milun, M.; Fukutani, K. Acceleration of Hydrogen Absorption by Palladium through Surface Alloying with Gold. *Proc. Natl. Acad. Sci.* **2018**, *115*, 201800412.

(64) Boon-Brett, L.; Bousek, J.; Black, G.; Moretto, P.; Castello, P.; Hübert, T.; Banach, U. Identifying Performance Gaps in Hydrogen Safety Sensor Technology for Automotive and Stationary Applications. *Int. J. Hydrogen Energy* **2010**, *35*, 373–384.

(65) Dahlin, A. B.; Tegenfeldt, J. O.; Höök, F. Improving the Instrumental Resolution of Sensors Based on Localized Surface Plasmon Resonance. *Anal. Chem.* **2006**, *78*, 4416–4423.

(66) Nyberg, C.; Tengstål, C. G. Adsorption and Reaction of Water, Oxygen, and Hydrogen on Pd(100): Identification of Adsorbed Hydroxyl and Implications for the Catalytic H_2 –O_2 Reaction. *J. Chem. Phys.* **1984**, *80*, 3463–3468.

(67) Yang, F.; Kung, S.-C.; Cheng, M.; Hemminger, J. C.; Penner, R. M. Smaller Is Faster and More Sensitive: The Effect of Wire Size on the Detection of Hydrogen by Single Palladium Nanowires. *ACS Nano* **2010**, *4*, 5233–5244.

(68) Yang, F.; Taggart, D. K.; Penner, R. M. Fast, Sensitive Hydrogen Gas Detection Using

Single Palladium Nanowires That Resist Fracture. *Nano Lett.* **2009**, *9*, 2177–2182.

(69) Yoo, H.-W.; Cho, S.-Y.; Jeon, H.-J.; Jung, H.-T. Well-Defined and High Resolution Pt Nanowire Arrays for a High Performance Hydrogen Sensor by a Surface Scattering Phenomenon. *Anal. Chem.* **2015**, *87*, 1480–1484.

(70) Burton, J. J.; Hyman, E.; Fedak, D. G. Segregation in Alloys. *J. Catal.* **1975**, *37*, 106–113.

(71) Ulvestad, A.; Welland, M. J.; Cha, W.; Liu, Y.; Kim, J. W.; Harder, R.; Maxey, E.; Clark, J. N.; Highland, M. J.; You, H.; *et al.* Three-Dimensional Imaging of Dislocation Dynamics during the Hydriding Phase Transformation. *Nat. Mater.* **2017**, *16*, 565–571.

(72) Rousset, J. L.; Bertolini, J. C.; Miegge, P. Theory of Segregation Using the Equivalent-Medium Approximation and Bond-Strength Modifications at Surfaces: Application to Fcc Pd- *X* Alloys. *Phys. Rev. B* **1996**, *53*, 4947–4957.

(73) Løvvik, O. M. Surface Segregation in Palladium Based Alloys from Density-Functional Calculations. *Surf. Sci.* **2005**, *583*, 100–106.

(74) Hübert, T.; Boon-Brett, L.; Palmisano, V.; Bader, M. A. Developments in Gas Sensor Technology for Hydrogen Safety. *Int. J. Hydrogen Energy* **2014**, *39*, 20474–20483.

(75) *U.S. Department of Energy, Energy Efficiency and Renewable Energy (EERE), Fuel Cell Technologies Office. Multi-Year Research, Development, and Demonstration Plan, 2011-2020. Section 3.7 Hydrogen Safety, Codes and Standards*; 2015.

(76) *U.S. Department of Energy, Hydrogen, Fuel Cells & Infrastructure Technologies Program. Multi-Year Research, Development, and Demonstration Plan, 2003-2010.*

Section 3.4 Fuel Cells; 2005.

(77) Koo, W.-T.; Qiao, S.; Ogata, A. F.; Jha, G.; Jang, J.-S.; Chen, V. T.; Kim, I.-D.; Penner, R. M. Accelerating Palladium Nanowire H2 Sensors Using Engineered Nanofiltration. *ACS Nano* **2017**, *11*, 9276–9285.

(78) Jeon, K.-J.; Moon, H. R.; Ruminski, A. M.; Jiang, B.; Kisielowski, C.; Bardhan, R.; Urban, J. J. Air-Stable Magnesium Nanocomposites Provide Rapid and High-Capacity Hydrogen Storage without Using Heavy-Metal Catalysts. *Nat. Mater.* **2011**, *10*, 286–290.

(79) Gong, C.; Leite, M. S. Noble Metal Alloys for Plasmonics. *ACS Photonics* **2016**, *3*, 507–513.

(80) Kadkhodazadeh, S.; Nugroho, F. A. A.; Langhammer, C.; Beleggia, M.; Wagner, J. B. Optical Property–Composition Correlation in Noble Metal Alloy Nanoparticles Studied with EELS. *ACS Photonics* **2019**, *6*, 779–786.

(81) Nugroho, F. A. A.; Diaz de Zerio Mendaza, A.; Lindqvist, C.; Antosiewicz, T. J.; Müller, C.; Langhammer, C. Plasmonic Nanospectroscopy for Thermal Analysis of Organic Semiconductor Thin Films. *Anal. Chem.* **2017**, *89*, 2575–2582.

(82) Sauerbrey, G. Verwendung von Schwingquarzen Zur Wägung Dünner Schichten Und Zur Mikrowägung. *Zeitschrift für Phys.* **1959**, *155*, 206–222.

TOC Only